Directional propagation channel estimation and analysis in urban environment with panoramic photography

Jean-Marc Conrat, Patrice Pajusco

Directional Propagation Channel Estimation and Analysis in urban Environment with Panoramic Photography

Jean-Marc Conrat[1], Patrice Pajusco[2],

[1] Orange Labs, Wireless Engineering Propagation, 6. av des Usines, 90007 Belfort Cedex

[2] Télécom Bretagne Lab-STICC, Technopole Brest Iroise, CS83818, 29238 Brest Cedex 03

This article aims to provide readers with a physical understanding of the propagation channel that is complementary to the mathematical channel modeling. It presents an analysis of the directional propagation channel based on radiophotos. Radiophotos are graphical objects where directions of arrival are superimposed on 3D panoramic photographs. The interaction between EM waves and the environment is immediately identified with these representations. This paper focuses on the direction of arrival at mobile in an urban macrocell environment. The first radiophoto collection illustrates the major propagation phenomena such as the reflection, the diffraction or the street canyoning. The second collection illustrates typical propagation channel profiles that are classified according to the delay, azimuth and elevation spread values. The paper also describes an original panoramic based method for estimating the noise level in the azimuth-elevation domain.

Keywords:

Corresponding author: J.M. Conrat; email: jeanmarc.conrat@orange-ftgroup.com; phone: +33 3 84 54 42 68

I. INTRODUCTION

Growing demand for high-speed wireless networks has led to the development of new, more sophisticated radio interfaces. In particular, multi-antenna (MIMO) technology has recently emerged to increase system performance while limiting spectral resource utilization [1, 2]. As with any other modern radio interface, development, testing and evaluation of MIMO systems involve extensive computer simulations. Accurate and reliable propagation channel models are therefore required in order to obtain coherent results from the entire simulation chain [3]. Modeling is always preceded by propagation channel characterization. In fact, channel models cannot be defined without the physical understanding of the measurement data. For example, [4] and [5] present characterisation results in urban areas, such as the identification of reflection/diffraction/diffusion by buildings. However, the measurement physical interpretation is sometimes long and laborious. Simultaneous comparison of measurement results, measurement campaign notes, building or city maps, and standard photographs is time-consuming and can be a source of error. Development of efficient and simple

measurement analysis tools is therefore a concern for scientists involved in propagation channel characterisation.

Mixing measurement results with environment photographs is certainly the most convenient way to physically analyse propagation channel behaviour. In 2002, photographs taken with a standard lens onto which representative rays detected by the SAGE algorithm were superimposed, were included in [6]. More recently, a method based on panoramic images generated from 6 video streams was presented in [7]. Omnidirectional video data that were captured during the measurements were used in combination with the measurement results to identify and relate the received radio waves directly to the actual environment. Both analyses were limited to the campus environment with large building separation.

The purpose of this paper is to extend the previous analyses for real urban macrocell environments. The physical interpretation will be based on radiophotos which are defined as the superimposition of 3D panoramic photos, with directions of arrival at the mobile (MS-DoA). 3-D panoramic photos are images with an angle of view that reaches 180° vertically and 360° horizontally. A radiophoto example is given in Figure 1. The 0° azimuth axis represents the BS-MS (base station-mobile station) line. Each path is represented by a circle, the radius or colour of which is proportional to its power.

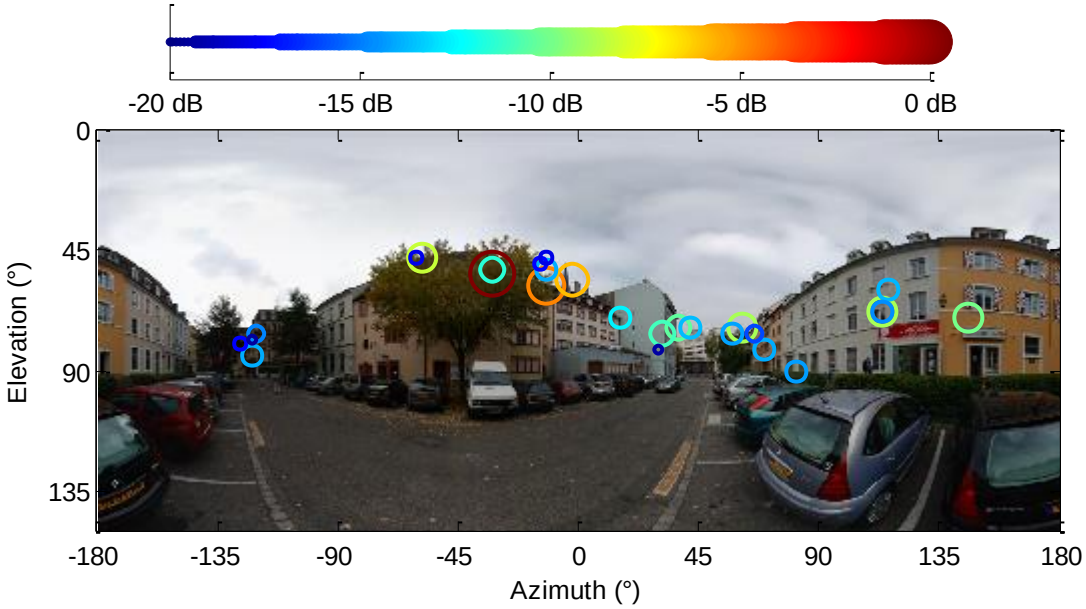

Figure 1: Radiophoto example

The paper is organized as follow: the second section describes the measurement campaign and the directional propagation channel estimation method. An original method based on radiophotos is applied in order to detect and suppress the noise in the azimuth–elevation domain. The third section shows a large collection of radiophotos highlighting the main physical phenomena involved in the propagation channel in outdoor urban environment. Section 3 also provides radiophotos related to typical measurement files. The typical file selection was achieved according to the azimuth, elevation and delay spread values.

II. MEASUREMENT DATA

A) Measurement campaign description

The measurement campaign was conducted in the city centre of Mulhouse, France, where the average height of buildings is about 25 meters. The propagation channel complex impulse responses (CIR) were collected with the wideband channel sounder of Orange Labs (AMERICC) [8] at a carrier frequency of 2.2 GHz and a measurement bandwidth of 62.5 MHz. The Tx antenna was placed on the rooftop of a building at about 30 meters above ground level. The Tx antenna was a 12 dBi gain sectorial antenna with a half power elevation beamwidth of 16 °. The transmitted power was 43 dBm. Figure 3 and Figure 4 show the urban environment viewed from the base station. At the receiver side, a static reference antenna and a Virtual Uniform Planar Array (VUPA) of 21×21 omni-directional dipole antennas were located on the roof of a car (Figure 2). The signal coming from the reference antenna was used for time and phase synchronisation. The synchronisation procedure is detailed in [9, 10]. The Tx and Rx antennas were dual-polarized, however, this paper deals only with the results in vertical polarization. A polarization statistical analysis based on this measurement campaign is presented in [11]. Rx1 to Rx10 in Figure 3 and Figure 4 indicate some Rx locations, the measurement results of which will be discussed in the following next sections.

Figure 2: Receiving and transmitting antennas

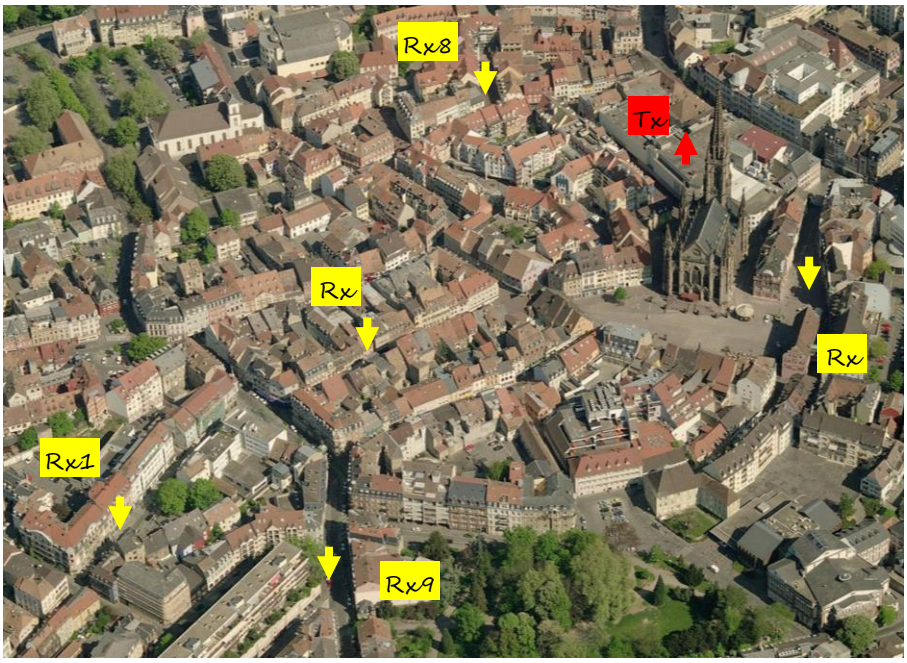

Figure 3: Base station aerial view 1

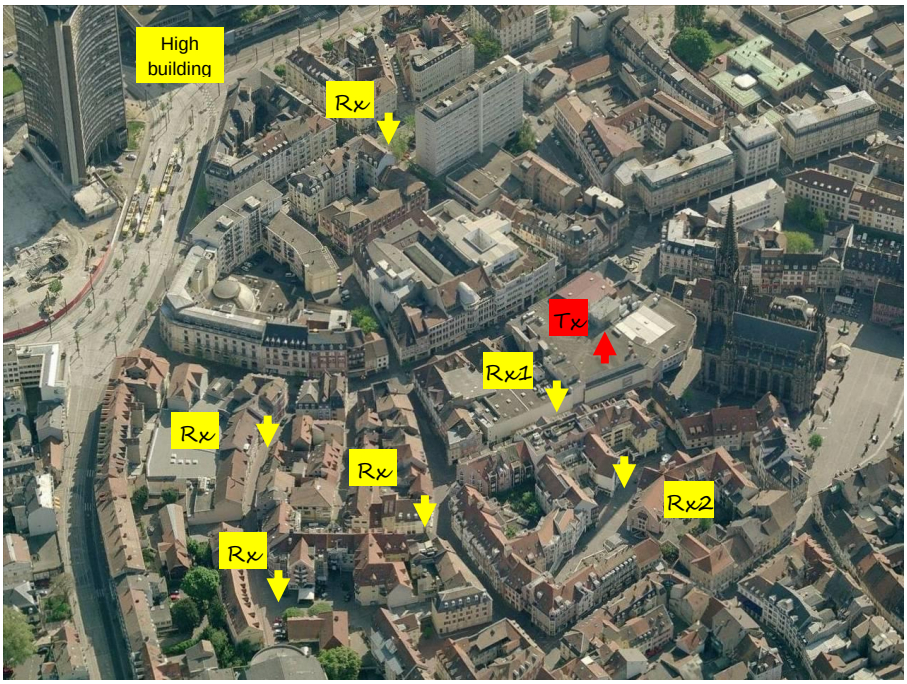

Figure 4: Base station aerial view 2

B) Beamforming processing

A Bartlett beamforming algorithm is used to compute the various directions of arrival at the receiver. The general principle is to synthesize a narrow-beam antenna and scan the environment in all directions. The beamforming algorithm is applied at each delay and the final result is the directional impulse response $h(\theta,\varphi,\tau)$, where θ, φ, τ are the elevation, the azimuth and the delay respectively. $h(\theta,\varphi,\tau)$ is computed by applying the following formula:

$$h(\theta,\varphi,\tau) = \frac{\sum_{m}^{NbAntRow} \sum_{n}^{NbAntLine} \left(h_{mn}(\tau) \cdot \overline{B_{mn}(\theta,\varphi)} \cdot W_{mn} \right)}{G_{BS} \cdot G_{MS}(\theta,\varphi) \cdot \sum_{m}^{21} \sum_{n}^{21} W_{mn}} \quad (1)$$

With

$h_{mn}(\tau)$:	Impulse response at position *(m,n)* in the VUPA
G_{BS} :	Tx antenna gain in the Tx-Rx direction
$G_{MS}(\theta, \varphi)$:	Rx antenna gain in direction (θ, φ)
$B_{mn}(\theta, \varphi)$:	Antenna array response in direction (θ, φ)
W_{mn} :	Weighting function
NbAntRow,	VUPA row number
NbAntLine:	VUPA line number. For the described campaign, *NbAntLine=NbANtRow= 21*

W_{mn} is a 2-dimensional weighting function which reduces the sidelobe level. The amplitude normalization complies with the following condition: If the VUPA is impinged by a ray with an amplitude A and a direction (θ,φ), the amplitude estimated by the beamformer in direction (θ,φ) is A. Results presented in the next sections use the Hanning function.

The beamforming algorithm is limited to a delay interval that includes CIR non-noisy parts. The noise level is estimated with the minimum of the maximum (MinMax) method illustrated in Figure 5. The CIR is divided in N segments. P_{max}^{i} is the maximum power over segment i. The noise level P_{noise} is equal to:

$$P_{noise} = \min_{i=1,N} \left(P_{max}^{i} \right) + margin \quad (2)$$

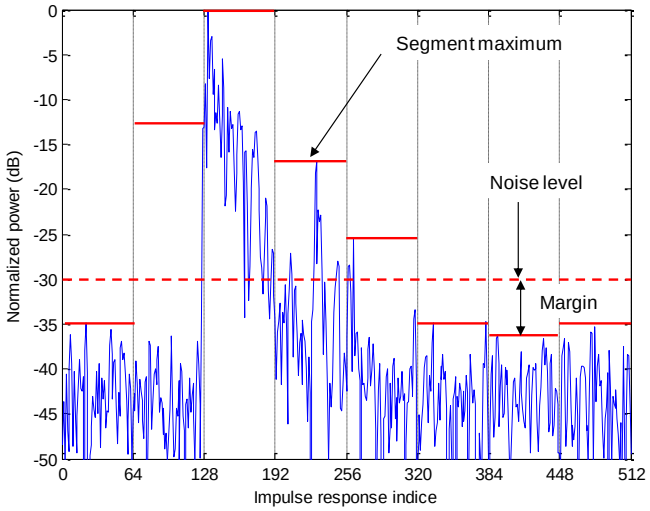

Figure 5: Impulse response noise estimation with 8 segments

Margin compensates the possible difference between the MinMax value and the maximum of noisy segments. The segment number and the margin are manually evaluated from a few CIRs and then applied to all CIRs. The MinMax method is simple and efficient but assumes that a non-neglictible part of the impulse response is noise. This assumption is usually checked as channel sounder excitation sequences are selected much longer than the expected maximal CIR length. A MinMax method adaptation in the azimuth-elevation domain is presented in paragraph II.C).

The VUPA horizontal planar symmetry introduces an up/down ambiguity in the elevation estimation. From a strictly theoretical point of view, two rays with the same azimuth but with supplementary elevation angles cannot be resolved. Practically, the metallic plate, on which the XY-rail is set, shadows paths coming from the bottom. We can therefore assume that the measurement system is able to estimate without ambiguity elevations between 0° and 90°. Elevation 0° is the vertical direction.

In order to visualize $h(\theta,\varphi,\tau)$ clearly, different power profiles are defined as mentioned in Table 1. Examples of power profiles are shown in Figure 6.

Table 1: Profile definitions

Delay Power Profile (DPP)	$DPP(\tau)=\sum_{\theta}\sum_{\varphi}\left\|h(\theta,\varphi,\tau)\right\|^2$
Azimuth Elevation Power Profile (AEPP)	$AEPP(\theta,\varphi)=\sum_{\tau}\left\|h(\theta,\varphi,\tau)\right\|^2$
Azimuth Delay Power Profile (ADPP)	$ADPP(\varphi,\tau)=\sum_{\theta}\left\|h(\theta,\varphi,\tau)\right\|^2$

Elevation Delay Power Profile (EDPP)	$EDPP(\theta,\tau)=\sum_{\varphi}\left\|h(\theta,\varphi,\tau)\right\|^2$
Azimuth Power Profile (APP)	$APP(\varphi)=\sum_{\theta}\sum_{\tau}\left\|h(\theta,\varphi,\tau)\right\|^2$
Elevation Power Profile (EPP)	$EPP(\theta)=\sum_{\varphi}\sum_{\tau}\left\|h(\theta,\varphi,\tau)\right\|^2$

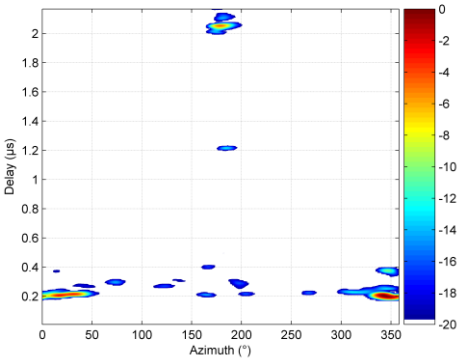

(a) ADPP

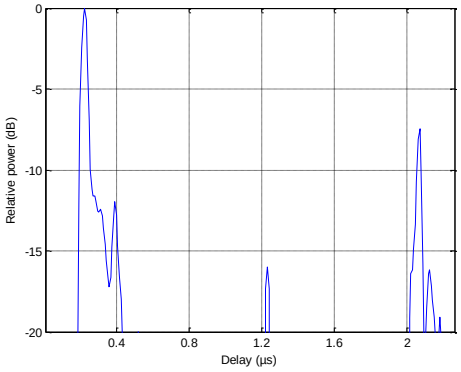

(b) DPP

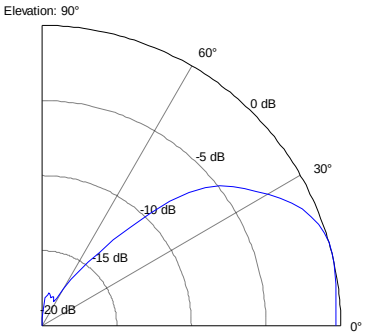

(c) EPP

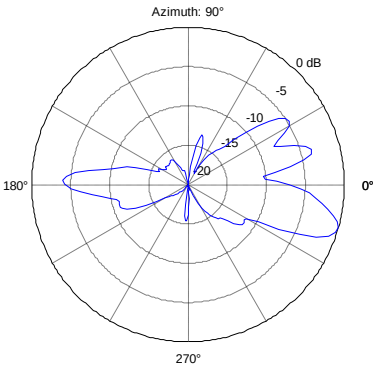

(d) APP

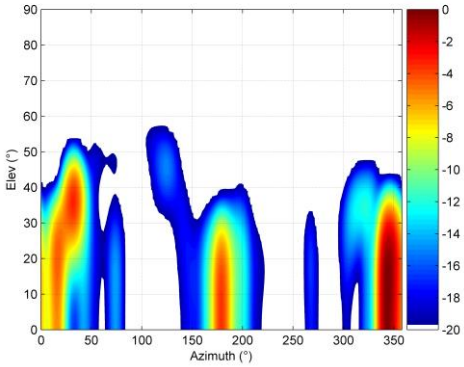

(e) AEPP

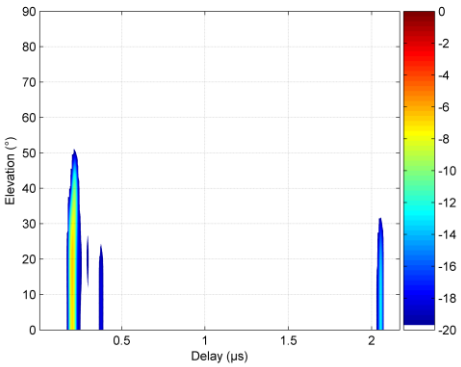

(f) EDPP

Figure 6: Power profiles computed from the directional impulse response, location Rx10

C) Channel discretization

The discretization process consists in finding the local maxima of $|h(\theta,\varphi,\tau)|^2$ [12]. $h(\theta,\varphi,\tau)$ is converted in a set of ray defined by matrice *Ray*.

$$Ray = \left[P_i \ , \tau_i \ , \theta_{iMS} , \varphi_{iMS} \right] \qquad (3)$$

$P_i, \tau_i \ , \theta_i$ and φ_i are respectively, the power, the delay, the elevation and the azimuth of the i_{th} ray. The method is illustrated in Figure 7.

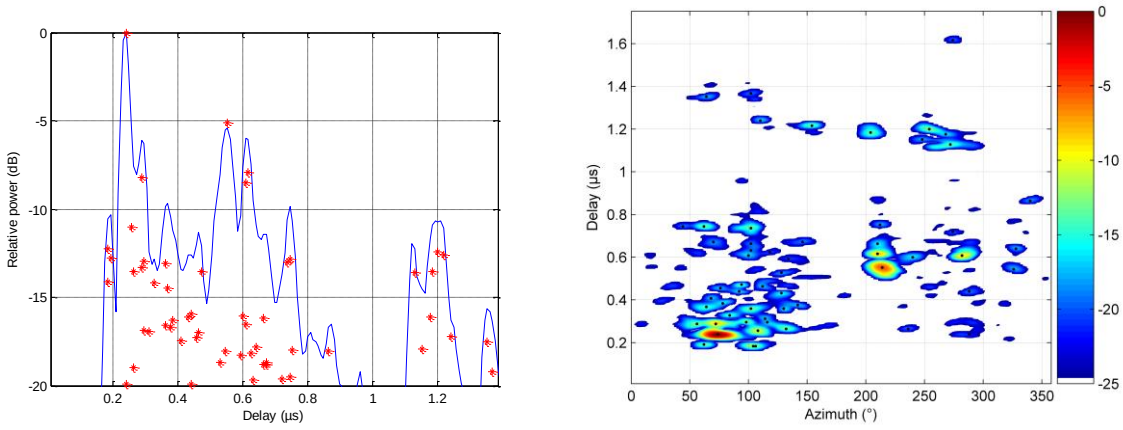

(a) DPP (b) ADPP

Figure 7: Path estimation via local maxima detection. Estimated paths are plotted with red crosses on the DPP plot and with dark points on the ADPP plot.

This new representation has several advantages. It dramatically reduces the size of data structures used for saving the results, the computational complexity of successive operations and therefore the computational time. On the other hand, retaining only the peak values from the continuous profiles intrinsically ignores the width of the beamformer main lobe (along the angular dimension) and the measurement equipment rise time (along the temporal dimension).

The noise level determination is a crucial step in the channel estimation method described above. The noise includes all undesirable signals due to the thermal noise, beamforming sidelobes, measurement equipment limits or channel non-stationarity. Regarding the path estimation process described in the previous paragraphs, the noise level defines a threshold above which local maxima detected on power profiles are not considered as physical paths. Its minimal value is theoretically bounded by the estimator space-time sidelobes. The directional impulse response was computed using a Hanning function. Therefore all maxima, the power of which is lower than the maximal power minus 30 dB, are withdrawn from the estimation. Its maximal value depends on the measurement conditions and is calculated for each impulse response delay by the MinMax method extended in the azimuth-elevation domain.

For each delay, $h(\theta,\varphi,\tau)$ is divided into $N_{elev}\times N_{azi}$ tules as shown in Figure 8. The noise level $P_{noise\_minmax}(\tau)$ is processed according equation (4). $P_{max}^{i,j}(\tau)$ is the maximum of $|h(\theta,\varphi,\tau)|^2$ over tule i,j at delay τ.

$$P_{noise\_minmax}(\tau) = \min_{i=1,N_{elev}\ j=1,N_{azi}} \left(P_{max}^{i,j}(\tau)\right) + margin \qquad (4)$$

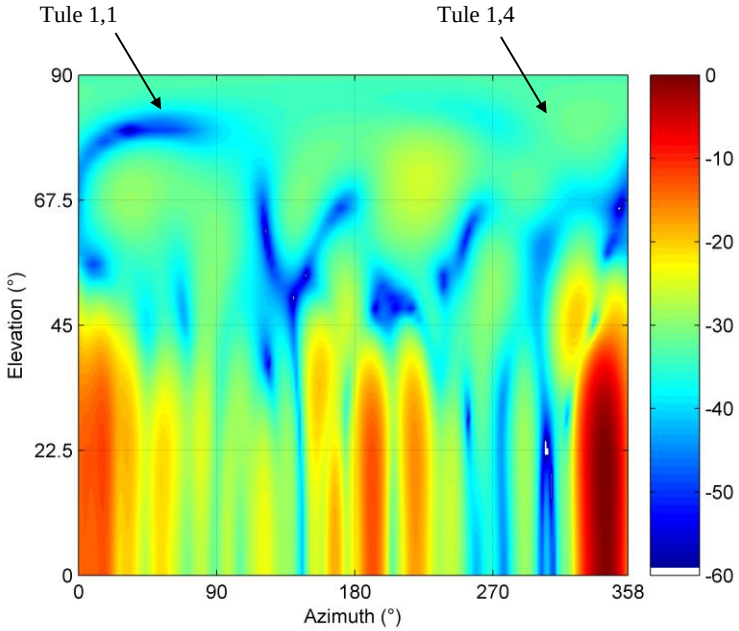

Figure 8: Tule division example

As pointed out in paragraph II.B), the MinMax method is efficient if N_{elev}, N_{azi} and *margin* are correctly calibrated from a few measurement samples. The calibration consists in comparing $P_{noise\_minmax}(\tau)$ with a noise reference value called $P_{noise\_ref}(\tau)$ and calculated thanks the radiophoto. The method is based on two basic assumptions: Firstly, receiving power from the sky is physically impossible. There can be obstacles above the vehicle momentarily, but the obstacle shadowing elevation is practically always lower than the building shadowing elevation as shown in Figure 9. Secondly, the noise is statistically not dependant on the direction of arrival. A sky area is defined inside a panoramic photo where no signal can be received. The maximum power within the sky area gives $P_{noise\_ref}(\tau)$.

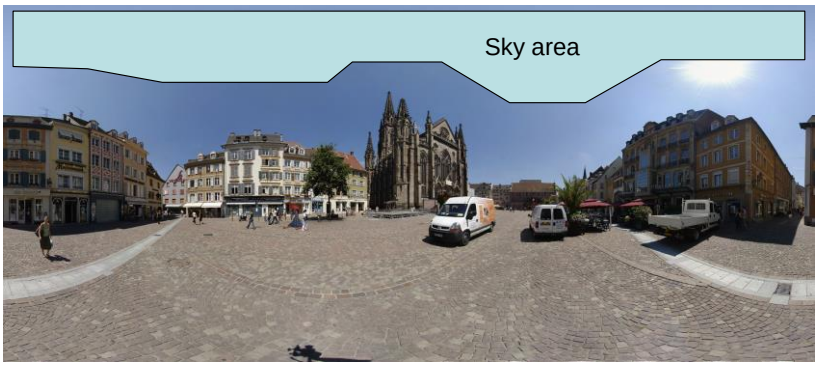

Figure 9: Sky area example

The optimal values for N_{elev}, N_{azi} are those that minimize the peak-to-peak value of $P_{noise\_minmax}(\tau)$-$P_{noise\_ref}(\tau)$. Typical N_{elev}, N_{azi} and *margin* values are respectively 4, 4 and 10 dB. Performance of noise estimation methods are illustrated in Figure 10. The curve denoted *Max* is equal to the maximum of $|h(\theta,\varphi,\tau)|^2$ at delay τ. The curve denoted MinMax is $P_{noise\_minmax}(\tau)$ minus *margin*. The directional impulse response depicted in Figure 8 was computer at delay 0.28 µs.

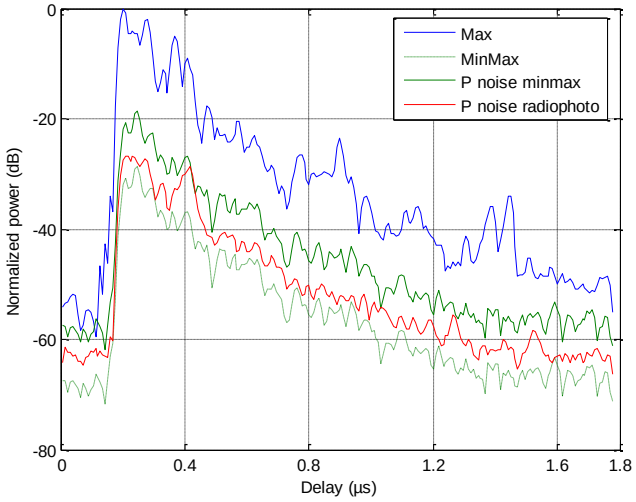

Figure 10: Noise estimation as a function of delay, N_{elev} = 4, N_{azi} = 4, *margin* = 10 dB

The accuracy of the path estimation method was evaluated by selecting measurement points in Line-of-Sight condition. The main path is defined as the path with the lowest attenuation. As there is no obstacle between Tx and Rx, the main path is the direct path between Tx and Rx. The main path direction was compared with the direction computed from the Rx and Tx coordinates and the main path attenuation was compared to the free space loss attenuation. The angular difference is less than 5° and the attenuation difference is less than 4 dB. The angular difference is not significant as it depends on the Tx and Rx coordinate accuracy as well. The attenuation difference is explained by the addition of small errors on the Tx power, antenna gains or cable losses but it is impossible to characterize all sources of error separately. Nevertheless, even though the path estimation may be locally biased, the measurement data and estimation process are enough accurate and reliable for understanding propagation channel physical phenomena.

D) Radiophoto generation

Panoramic photography is a style of photography that aims to create images with wide fields of view. When the angle of view reaches 180° vertically and 360° horizontally, panoramic photos are called 3-D panoramic photos. The easiest way to obtain such photos is the stitching method. The principle is to take a set of photographs that overlap slightly and to stitch them with specific software. The main drawback is the relatively long acquisition time, about ten minutes, which prohibits all real-time applications. However, consumer products can be used.

Therefore, the stitching method is the most widely used and a lot of information related to the equipment or software is available on the web. The equipment is composed of a conventional digital camera, a fish-eye lens, a tripod and a panoramic head. The fish-eye lens is a very wide-angle lens. The panoramic head is mounted on a tripod (Figure 11) and has two functions: to set the axis of rotation precisely and to rotate the camera in 3-D. Panoramic photography is performed in three steps:

- Panoramic head setting:

The panoramic head should be set in order to match up the entrance pupil of the lens (optical focalisation point) with the rotation centre of the panoramic head. An accurate setting avoids parallax errors and makes image stitching easier. The entrance pupil is located on the lens rotation axis but its exact location is unknown, as lens manufacturers refuse to disclose this data, deeming it confidential. Fortunately, there are very simple methods to adjust the panoramic head.

- Photo acquisition:

First, the number of photographs needed to cover the selected area is calculated. This number depends on the lens angular aperture and on the overlapping rate. The overlapping rate indicates the percentage of common field of view between two consecutive pictures. It is generally considered that an overlapping rate of about 20-25% makes correct stitching possible. As a next step, photographs are shot. In real environments, the light level changes greatly and photographs taken into the sun tend to be over-exposed. In this case, increasing the overlapping rate helps the stitching software to generate a panoramic photo with uniform brightness.

- Picture stitching and panorama export:

The quality of this step depends heavily on the software. We used Stitcher Unlimited software that performs all operations automatically and efficiently. The most time-consuming parts of the processing are the image stitching between neighbouring pictures and the brightness smoothing. Once these operations are completed, the panoramic photography is generated according to a user-defined projection system. We used spherical projection, where the X axis is proportional to the azimuth and the Y axis proportional to the elevation.

Figure 12 gives an example of 24 shot at 2 elevations (0 ° and 45 °) and 12 azimuths (30 ° step). The overlapping rate is 50% horizontally and 70% vertically. This configuration leads to a panoramic photograph with a 360° horizontal angle of view and 155 ° vertical angle of view .

Figure 11: Camera set on the panoramic heading

Figure 12 : Set of photographs taken with the fish-eye lens

III. PHYSICAL ANALYSIS OF THE PROPAGATION CHANNEL

Locations Rx1 to Rx10 are depicted in Figure 3 and Figure 4.

A) Propagation mechanisms

Location Rx1 as shown in Figure 13 highlights two basic phenomena of electromagnetic waves propagation in outdoor environments: the reflection on building walls and the diffraction at horizontal building edges. Vertical building edges can also diffract the electromagnetic wave (Figure 14) although this phenomena is less frequent in macrocell environments where the transmit antenna is well above the rooftop level.

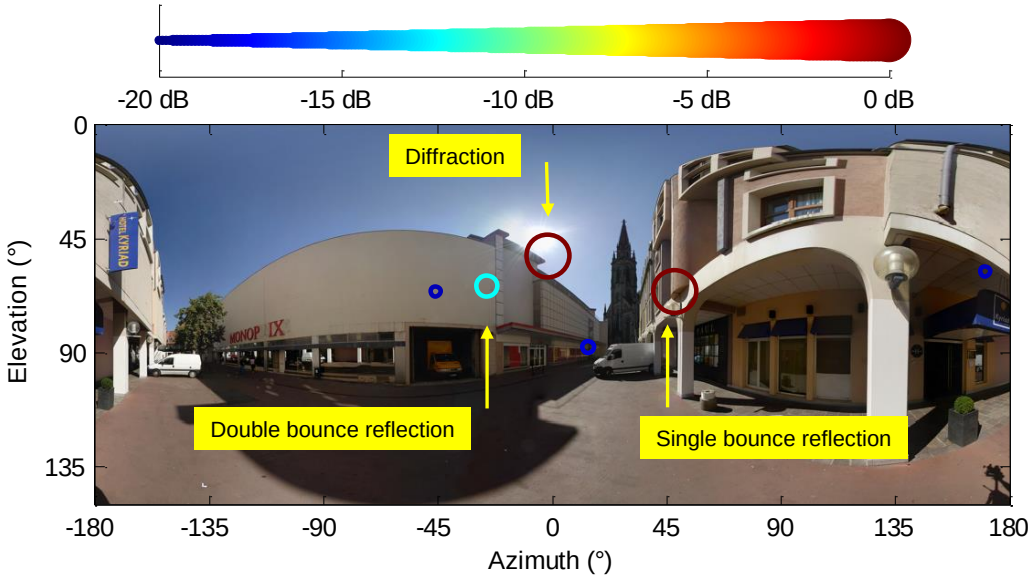

Figure 13: Radiophoto location Rx1

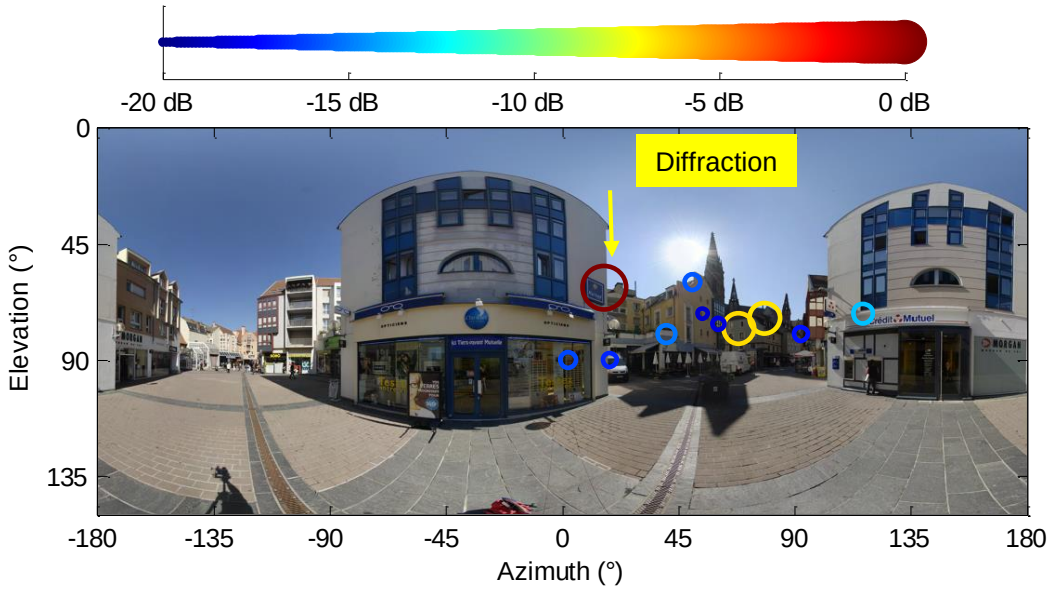

Figure 14: Radiophoto location Rx2

The first two examples were simple cases as the preponderant paths impinging the MS undergo less than 2 phenomena. Location Rx2 as shown in Figure 15 shows a much more complex case and illustrates the different propagation mechanisms that have also been described in [13-16].

Diffraction over Rooftops: Waves arrive at the MS from the rooftop level by diffraction at the edge of roofs. The direction of arrival is generally close to the BS-MS direction, the elevation may be high if the receiver is located near the wall of the building and the relative delays are short.

Street Guided Propagation: Waves arrive at the receiver at street level after travelling through street canyons by bouncing off walls along the street. Elevations associated with this mechanism are generally close to 90°.

Far Scatterer Reflection: Waves arrive at MS after reflection on a building, the height of which greatly exceeds the average rooftop level. A delay of about a few µs may be observed.

Miscellaneous: Other cases include reflection or diffraction on buildings or objects surrounding the MS.

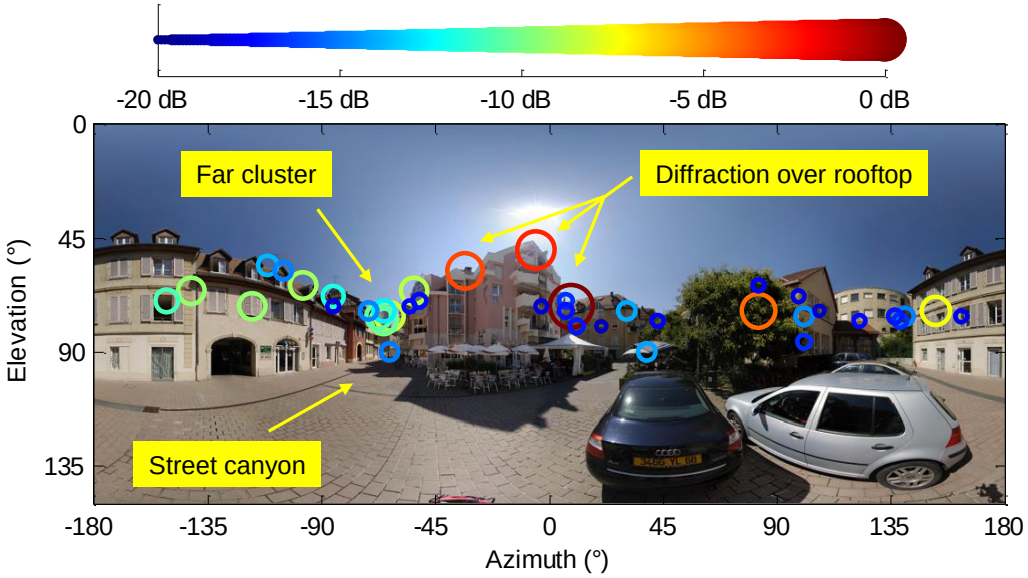

Figure 15: Radiophoto location Rx3

When the street axis corresponds to the BS-MS direction, the street canyon effect is enhanced as the different propagation mechanisms described above are combined to increase the received power in the street axis as shown in Figure 16. Similar results were reported in [13].

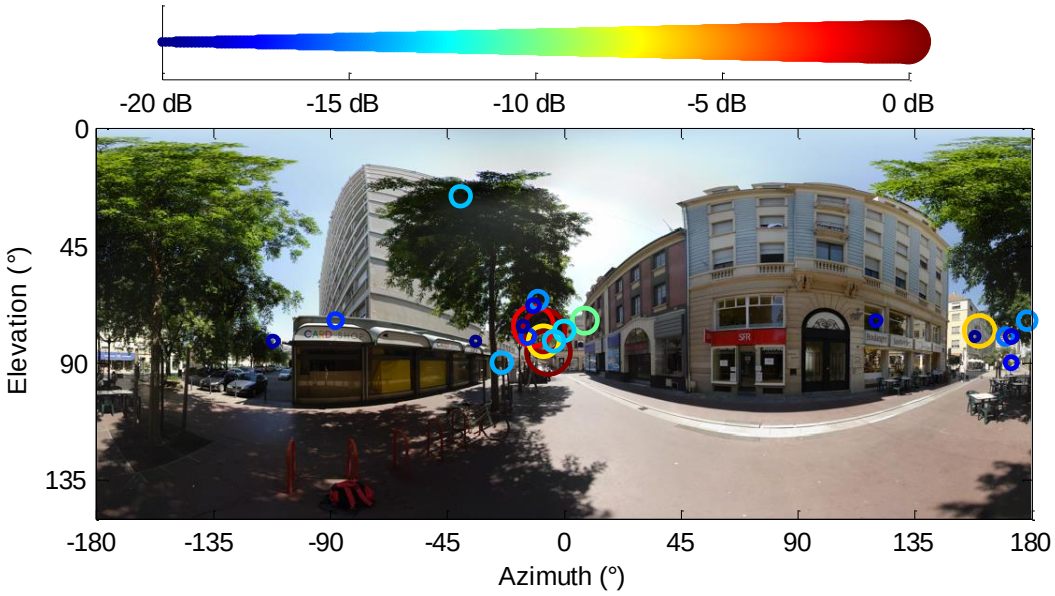

Figure 16: Radiophoto location Rx4

B) Typical propagation channels in an urban environment

Typical measurement files are selected according to the azimuth spread at mobile (*AS*), the elevation spread at mobile (*ES*) and the delay spread (*DS*). *AS* and *ES* indicate the spatial diversity degree of the propagation channel. *DS* indicates the frequential diversity degree. *AS*, *ES* and *DS* are key parameters for propagation channel characterization and modeling [17]. Therefore, they are appropriate channel metrics in order to identify typical propagation channels. *AS*, *ES* and *DS* are processed from the discrete representation of the continuous function $h(\theta,\varphi,\tau)$. Only rays within a dynamic range of 20 dB are considered in the spread processing. P_i, τ_i, θ_i and φ_i are respectively, the power, the delay, the elevation and the azimuth of the i_{th} ray.

DS and *ES* are calculated using equations (5) and (6)

$$DS = \sqrt{\frac{\sum_i (\tau_i - \bar{x})^2 \cdot P_i}{\sum_i P_i}} \quad \text{with} \quad \bar{x} = \frac{\sum_i \tau_i \cdot P_i}{\sum_i P_i} \qquad (5)$$

$$ES = \sqrt{\frac{\sum_i (\theta_i - \bar{x})^2 \cdot P_i}{\sum_i P_i}} \quad \text{with} \quad \bar{x} = \frac{\sum_i \theta_i \cdot P_i}{\sum_i P_i} \qquad (6)$$

AS is calculated according to equation (7) and complies with the 3GPP specification [18]

$$MS\text{-}AS = \min_{\Delta=1..2\pi}\left(AS(\Delta)\right) \text{ with } AS(\Delta) = \sqrt{\frac{\sum_i \left(\text{mod}(\varphi_i + \Delta) - \bar{x}\right)^2 \cdot P_i}{\sum_i P_i}} \text{ with } \bar{x} = \frac{\sum_i \text{mod}(\varphi_i + \Delta) \cdot P_i}{\sum_i P_i} \quad (7)$$

Mod designed the modulo-2π function.

The minimum and maximum spread values are analytically calculated in case of an equally powered azimuth distribution ranged in the interval [0,α]. Spread values ranged from 0 to $\alpha/\sqrt{12}$. For instance, *AS* ranges from 0° to 104° and ES ranges from 0° to 28°.

Before the typical measurement file selection itself, *AS*, *ES*, *DS* mean values are compared with those extracted from similar measurement campaigns and reported in Table 2. The carrier frequency ranged between 2 and 6 GHz and the measurement setup enabled direction of arrival estimation at MS. The environment was the outdoor macrocell environment and corresponds to scenario C2 defined by the WINNER European project [17]. Results are almost homogeneous, despite the fact that measurements have been performed in different European or Asian cities with a specific architecture or urban density. With the exception of extreme values, *DS* mean values range from 100 ns to 300 ns, *AS* mean values are within 50 and 70° and *ES* is about 8°. Therefore, typical propagation channels described below are not strongly specific to the measurement campaign environment and may be generalized to many types of urban areas.

Table 2: Measurement campaign summary

Place	Distance (m)	Bandwidth (MHz)	Carrier freq. (GHz)	DS (ns)	AS-MS (°)	ES-MS (°)	Ref.
Bristol	1500	20	2	300	73.6	NA	[19]
Helsinki	NA	60	5.3	NA	52.3	7.7	[20]
Stockholm	100	200	5.25	250	80	20	[21]
Helsinki	800	100	5.3	80-220	48	NA	[22]
Seoul	500	100	3.7	770	72	NA	[23]
Beijing	1000	100	2.35	210	65	NA	[24]
Illmenau	500	90	2.53	70	40	20	[25]
Winner C2	NA	100	2-6	230	52.5	NA	[17]

Mulhouse	500	62.5	2.2	170	55	7.6	Proposed

The typical propagation channel selection was done manually and based on a simple observation as shown in Figure 17: *ES* and *AS* are correlated, thereafter the measurement points may be classified according to their spatial diversity degree at MS. Three typical channels were defined: "Quasi-Los", "High Spatial Diversity" and "Standard". The first two typical channels are extreme cases that represent roughly 30 % of the measurement points. Furthermore, typical channels are not associated with the BS-MS distance. This statement is motivated both by the joint radiophoto and aerial view visual inspection and by the low correlation between the BS-MS distance and *AS* or *ES* illustrated by Figure 18.

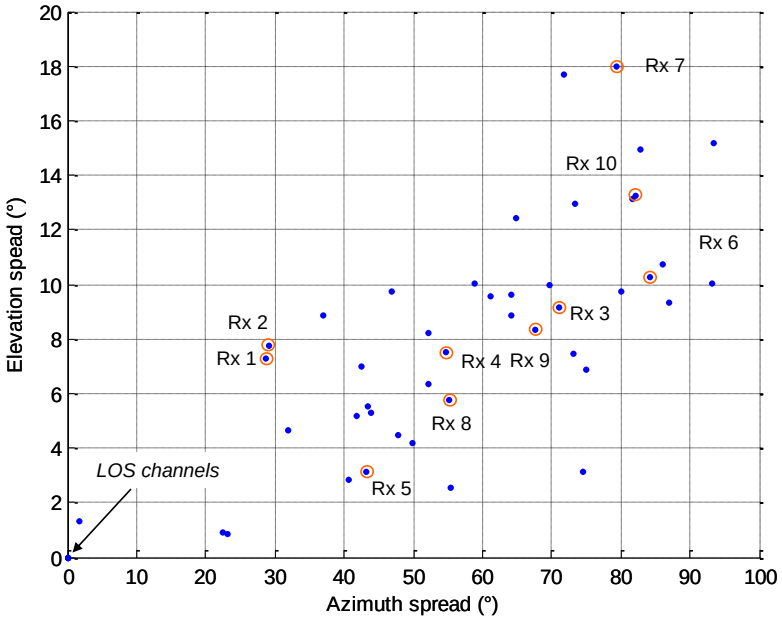

Figure 17: AS vs ES

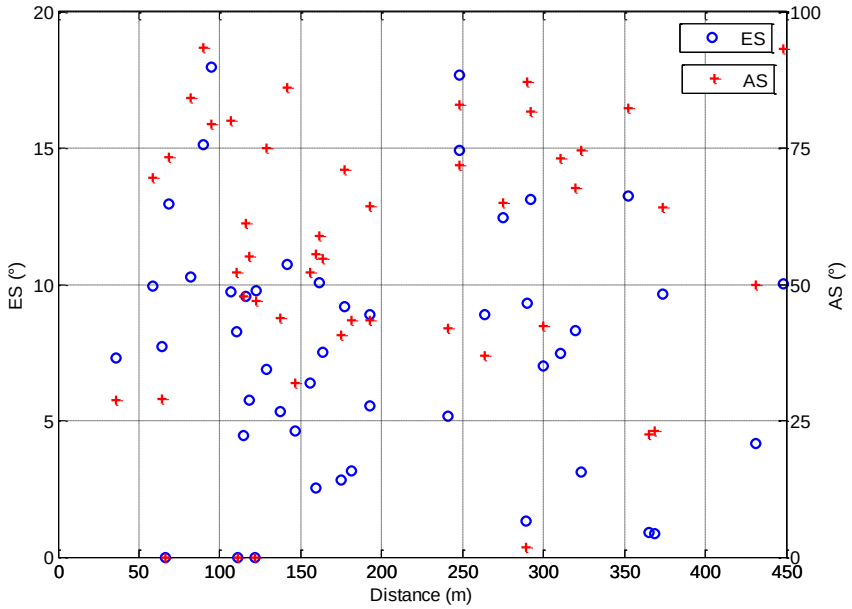

Figure 18: AS or ES relation with distance

Channel "Quasi-Los" (Figure 19): Propagation channels are usually classified as either LOS (line-of-sight) or NLOS (non-line-of-sight). Strictly speaking, LOS conditions mean that the transmitter is visible from the receiver. Channels with pure visibility are very rare in real urban environments but many situations classified as quasi-LOS have characteristics similar to LOS: a predominant path with a direction close to the line BS-MS and some weakened secondary paths less than 10 dB below the predominant path. The street axis has generally the same orientation as the line BS-MS. Delay spread values are centred around 30 ns and do not exceed 100 ns. AS ranges between a few and 50 degrees, depending on the secondary path azimuth.

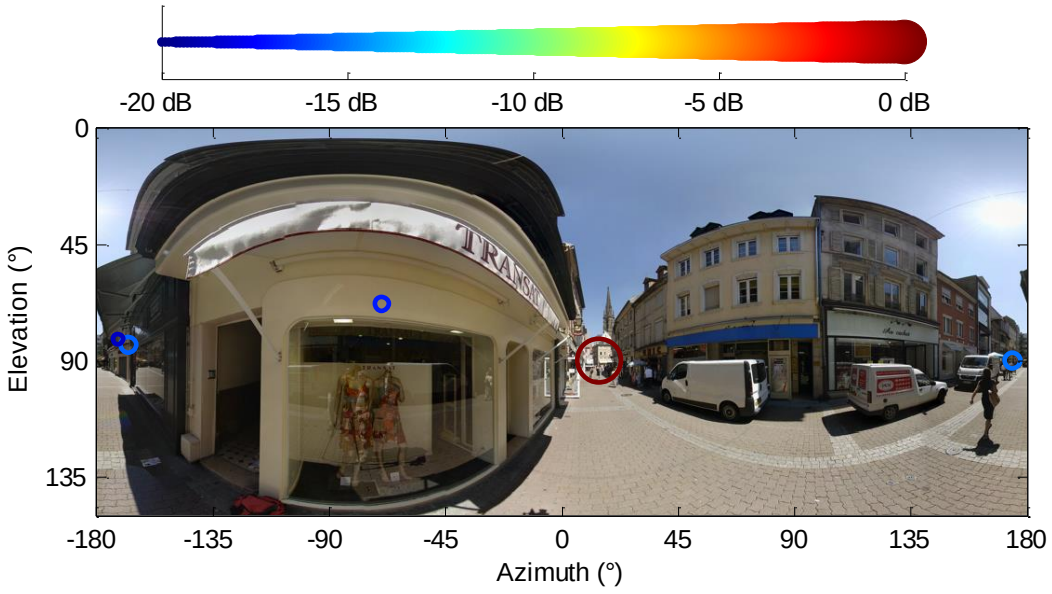

Figure 19: Radiophoto location Rx5

Channel "High spatial diversity" (Figure 20): The strongest path propagates less than 20% of the total received power. Some files exhibit a relatively high elevation spread. This occurs when two conditions are met as shown in Figure 21. Firstly, a high building is in the MS vicinity or the MS is close to the building wall. This geometrical configuration creates paths with an elevation ranged roughly between 40° and 70 °. Secondly, a significant part of the power arrives at MS with a low elevation. The addition of paths with low and large elevation creates ES close to 20°.

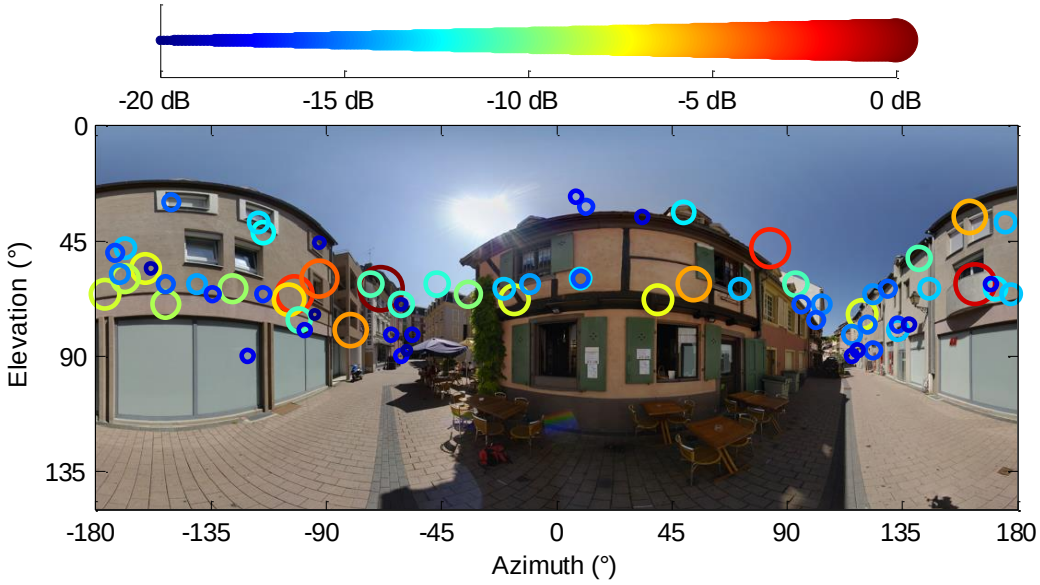

Figure 20: Radiophoto location Rx6

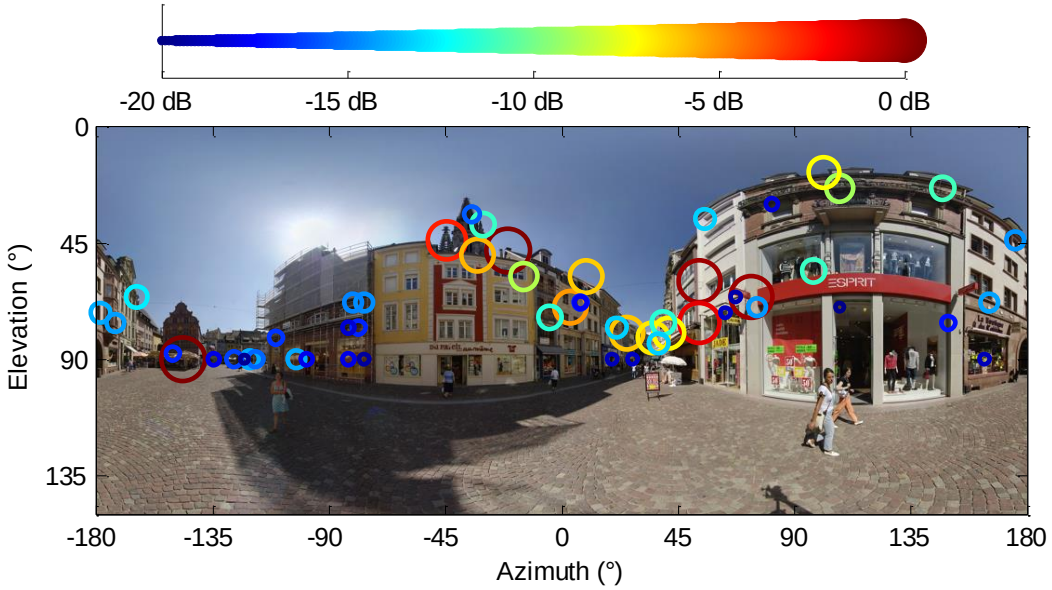

Figure 21: Radiophoto location Rx7

Channel "Standard": Except for some files that exhibit enhanced street canyon behaviour as described in section A), it is impossible to refine the selection as each measurement point is a particular case. Figure 22 and Figure 23 are two examples.

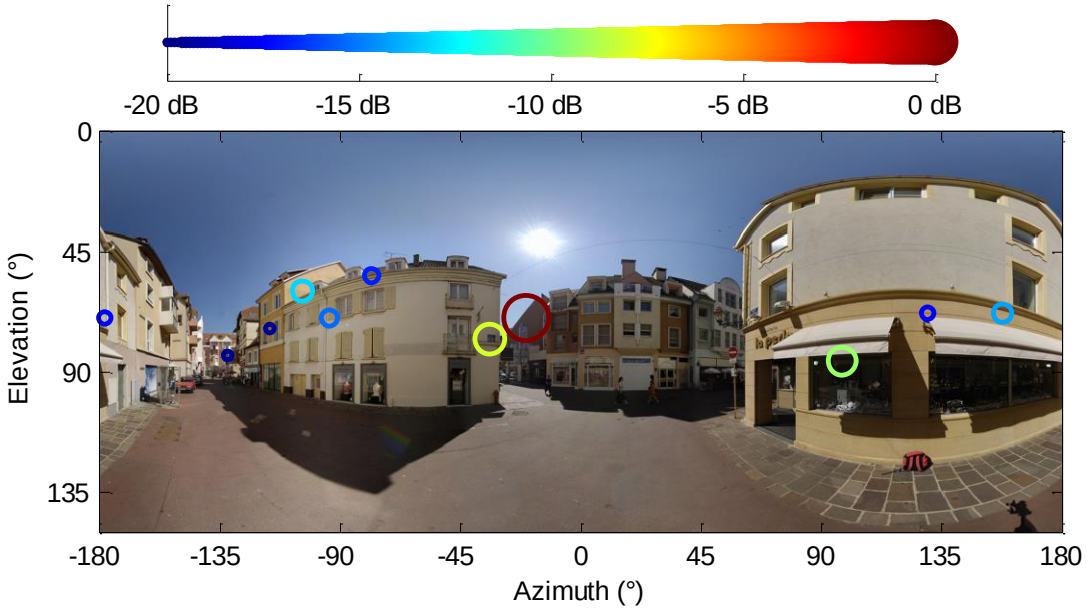

Figure 22: Radiophoto location Rx8

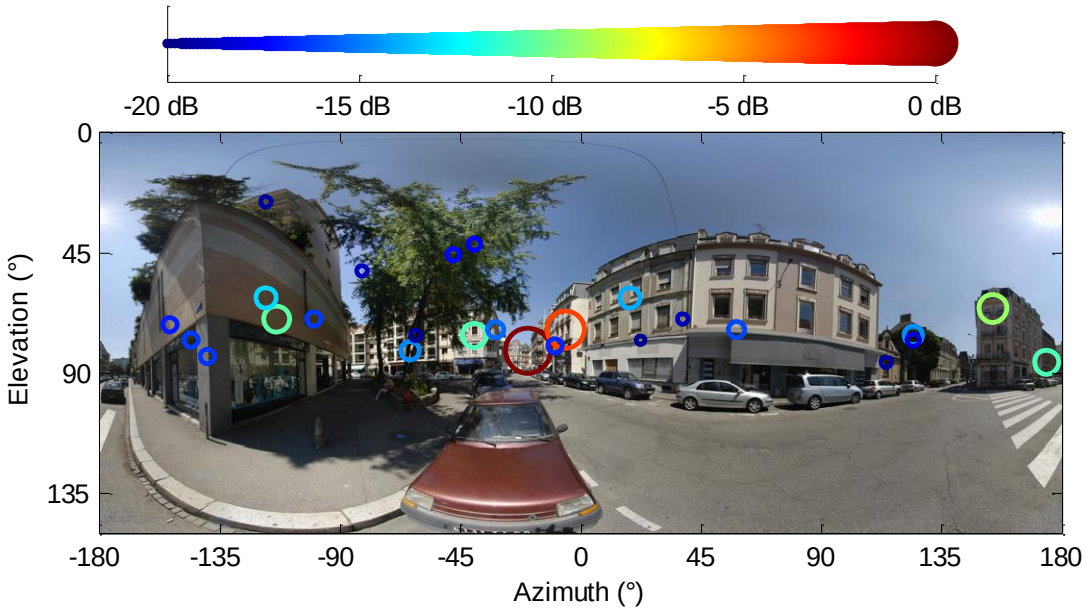

Figure 23: Radiophoto location Rx9

The groups "High spatial diversity" and "Standard" have the same mean DS value around 200 ns. Most of the DS are comprised between 30 ns and 400 ns but some files exhibit very large DS between 500 and 700 ns. This usual situation occurs when the impulse response is divided into two discontinuous parts as shown in Figure 24 and Figure 6. The first part is due to the interaction of the electromagnetic wave with the environment in the MS vicinity or close to

the line BS-MS. The second part is generally an interaction with a far building and generates paths with excess delay higher than 1.5 µs. This type of files agrees with environment C3 defined by the Winner project and labelled as "macro-cell bad urban ".

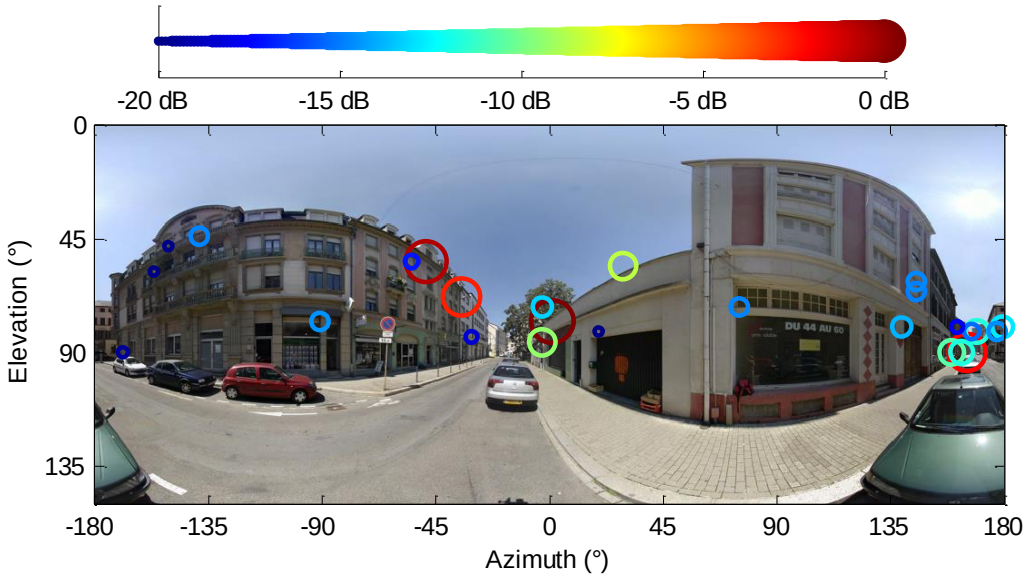

Figure 24: Radiophoto location Rx10

IV. CONCLUSION

The radiophoto examples given in this paper have shown the huge potential of radiophotos for propagation measurement data validation and analysis. In particular, the impact of the environment on the space-time propagation channel is immediately identifiable. Future work based on this technique will focus on the validation of simulation techniques, such as ray tracing or ray launching. Simulation results will be added to radiophotos, which should improve the understanding of the influence of geographical database accuracy on simulation reliability.

APPENDIX

Radiophotos do not provide any information about the path relative delay due to the intrinsic nature of the panoramic photo. However, the radiophoto principle can be extended to the video domain by generating radiovideos that show the AEPP time evolution dynamically. Radiovideos are multimedia documents that cannot be inserted in a journal paper but radiovideos related to the radiophoto examples given in this paper are available at http://perso.telecom-bretagne.eu/patricepajusco/jmwt/.

REFERENCES

[1] D. Gesbert, M. Shafi, S. Da-shan, P. J. Smith, and A. Naguib, "From theory to practice: an overview of MIMO space-time coded wireless systems," *IEEE Journal on Selected Areas in Communications*, vol. 21, pp. 281, 2003.

[2] A. Goldsmith, S. A. Jafar, N. Jindal, and S. Vishwanath, "Capacity limits of MIMO channels," *IEEE Journal on Selected Areas in Communications*, vol. 21, pp. 684, 2003.

[3] P. Almers, E. Bonek, A. Burr, and others, "Survey of Channel and Radio Propagation Models for Wireless MIMO Systems," *Eurasip Journal on Wireless Communications and Networking*, vol. 2007, Article ID 19070, 19 pages, 2007.

[4] M. Landmann, K. Sivasondhivat, J. I. Takada, I. Ida, and R. Thomä, "Polarization Behavior of Discrete Multipath and Diffuse Scattering in Urban Environments at 4.5 GHz," *Eurasip Journal on Wireless Communications and Networking*, vol. 2007, Article ID 57980, 16 pages, 2007.

[5] J. Laurila, K. Kalliola, M. Toeltsch, K. Hugl, P. Vainikainen, and E. Bonek, "Wideband 3D characterization of mobile radio channels in urban environment," *IEEE Transactions on Antennas and Propagation*, vol. 50, pp. 233, 2002.

[6] B. H. Fleury, P. Jourdan, and A. Stucki, "High-resolution channel parameter estimation for MIMO applications using the SAGE algorithm," International Zurich Seminar on Broadband Communications, Zurich, 2002.

[7] M. Kwakkernaat, Y. de Jong, R. Bultitude, and M. Herben, "High-Resolution Angle-of-Arrival Measurements on Physically-Nonstationary Mobile Radio Channels," *IEEE Transactions on Antennas and Propagation*, vol. 56, pp. 2720, 2008.

[8] J.-M. Conrat, P. Pajusco, and J. Y. Thiriet, "A Multibands Wideband Propagation Channel Sounder from 2 to 60 GHz," Instrumentation and Measurement Technology Conference (IMTC), Sorrento, 2006.

[9] A. Dunand and J.-M. Conrat, "Dual-Polarized Spatio-temporal Characterization in urban macrocells at 2 GHz," Vehicular Technology Conference (VTC - Fall), Baltimore, 2007.

[10] J.-M. Conrat, H. Dekov, M. Liénard, and N. Abdelmottaleb, "Analysis of the space-time Propagation Channel Behavior in Outdoor-to-Indoor Environment," Vehicular Technology Conference (VTC - Spring), Barcelone, 2009.

[11] A. Dunand and J.-M. Conrat, "Polarization behaviour in urban macrocell environments at 2.2 GHz," European Conference on Antenna and Propagation (EuCap), Edinburgh, 2007.

[12] J. M. Conrat and P. Pajusco, "Clusterization of the MIMO Propagation Channel in urban macrocells at 2 GHz," European Conference on Wireless Technology (ECWT), Paris, 2005.

[13] J. M. Conrat and P. Pajusco, "Typical MIMO propagation channels in urban macrocells at 2 GHz," European Wireless Conference (EW), Paris, 2007.

[14] K. Kalliola, H. Laitinen, P. Vainikainen, M. Toeltsch, J. Laurila, and E. Bonek, "3-D double-directional radio channel characterization for urban macrocellular applications," *IEEE Transactions on Antennas and Propagation*, vol. 51, pp. 3122, 2003.

[15] M. Toeltsch, J. Laurila, K. Kalliola, A. F. Molisch, P. Vainikainen, and E. Bonek, "Statistical characterization of urban spatial radio channels," *IEEE Journal on Selected Areas in Communications*, vol. 20, pp. 539, 2002.

[16] A. Kuchar, J. P. Rossi, and E. Bonek, "Directional macro-cell channel characterization from urban measurements," *IEEE Transactions on Antennas and Propagation*, vol. 48, pp. 137, 2000.
[17] "WINNER II channel models," IST Winner project - Phase II - D1.1.2, 2007.
[18] 3GPP, "Spatial Channel model for MIMO Simulations," *http://www.3GPP.org*, TR 25.996 V6.1.0., 2003.
[19] S. E. Foo, C. M. Tan, and M. A. Beach, "Spatial temporal characterization of UTRA FDD channels at the user equipment," Vehicular Technology Conference (VTC - Spring), Jeju, 2003.
[20] L. Vuokko, V.-M. Kolmonen, J. Kivinen, and P. Vainikainen, "Results from 5.3 GHz MIMO measurement campaign," COST 273 TD(04)193, Duisburg, 2004.
[21] J. Medbo, M. Riback, H. Asplund, and J.-E. Berg, "MIMO Channel Characteristics in a Small Macrocell measured at 5.25 GHz and 200 MHz Bandwidth," Vehicular Technology Conference (VTC - Fall), Dallas, 2005.
[22] T. Rautiainen, J. Juntunen, and K. Kalliola, "Propagation Analysis at 5.3 GHz in Typical and Bad Urban Macrocellular Environments," Vehicular Technology Conference (VTC - Spring), Dublin, 2007.
[23] J. J. Park, W. S. Kim, M. D. Kim, and H. K. Chung, "Measurement Results at 3.7 GHz in Urban Macrocell Environment," Vehicular Technology Conference (VTC - Fall), Baltimore, 2007.
[24] Z. Jianhua, D. Di, L. Yanping, N. Xin, G. Xinying, Z. Yu, H. Chen, and L. Guangyi, "Propagation characteristics of wideband MIMO channel in urban micro- and macrocells," International Symposium on Personal, Indoor and Mobile Radio Communications (PIMRC 2008), Cannes, 2008.
[25] C. Schneider, M. Narandzic, M. Kaske, G. Sommerkorn, and R. S. Thoma, "Large Scale Parameter for the WINNER II Channel Model at 2.53 GHz in Urban Macro Cell," Vehicular Technology Conference (VTC 2010-Spring), Taipei, 2010.

Bibliographies

Jean-Marc Conrat was born in Nancy, France, in 1968. He received the M.S. degree in electrical engineering from the Applied Science National Institut (INSA), Lyon, France, in 1991. Since 1993, he has been with Orange labs in Belfort, France. He is involved in propagation channel measurements, modeling and simulation. He started on wideband propagation channel studies for Land Mobile Satellite Systems (GLOBALSTAR). In 1996, he worked on the development of a new wideband channel sounder and was particularly involved in the software and digital parts. His current research interest is the characterization of the directional wideband propagation channel for terrestrial MIMO and cooperative communications.

 **Patrice PAJUSCO** received his Engineering degree from the Ecole Supérieure d'Electricité (SUPELEC) in Paris, in 1992. He joined the France Telecom research centre (CNET) in 1993, studying wideband propagation channel models for mobile communication systems and investigating wideband sounding techniques using antenna arrays. Starting in 1999, he was in charge of a team at Orange Labs working on propagation tools for wireless communication systems. In 2008, he joined Telecom Bretagne, where he is head of the microwave department. His main research interests are UWB and MIMO channel modeling.